buildings

Article

Insight into the Mechanical Performance of the TRECC Repaired Cementitious Composite System after Exposure to Freezing and Thawing Cycle

Fei Xu [1,2], Qi Li [3], Tongze Ma [2], Yao Zhang [1,2,*], Junwei Li [1] and Tao Bai [1,2]

1 Key Laboratory of Large Structure Health Monitoring and Control, Shijiazhuang Tiedao University, Shijiazhuang 050043, China; xufei@stdu.edu.cn (F.X.)
2 School of Safety Engineering and Emergency Management, Shijiazhuang Tiedao University, Shijiazhuang 050043, China
3 Shandong Hi-Speed Construction Management Group Co., Ltd., Jinan 250000, China
* Correspondence: zy201112212409@163.com

Abstract: Concrete structures are subjected to various forms of damage in cold regions. However, the interfacial bonding properties of traditional concrete (NC) reinforced with textile-reinforced cementitious composite (TRECC) under freeze–thaw cycle damage have not been fully studied. In this paper, different control groups were obtained by adjusting the types and layers of Fiber Reinforced Plastics (FRP) in TRECC and the interfacial roughness level between TRECC and NC. After experiencing 0–300 freeze–thaw cycles, each group underwent the uniaxial tensile test, three-point bending test, and scanning electron microscope observation. The results show that FRP type in TRECC can determine the strength of specimens. After 100 freeze–thaw cycles, the ultimate tensile strength of TRECC with two different FRP types increased by 38.4% and 55.3%, respectively, compared with TRECC. Furthermore, the bond strength and resistance to freeze–thaw damage of TRECC-NC interface increased with the increase of roughness under the action of freeze–thaw cycles. After 100 freeze–thaw cycles, the bonding strength of the repair system reached the highest. Compared with 0 freeze–thaw cycles, the ultimate tensile strength of the TRECC-NC reinforcement system under low roughness and high roughness increased by 50.05% and 61.25%, respectively. Meanwhile, the internal cracks of TRECC gradually developed and penetrated, reducing the cooperative working ability between TRECC-NC.

Keywords: TRECC; freezing and thawing cycle; TRECC-NC; FRP

check for updates

Citation: Xu, F.; Li, Q.; Ma, T.; Zhang, Y.; Li, J.; Bai, T. Insight into the Mechanical Performance of the TRECC Repaired Cementitious Composite System after Exposure to Freezing and Thawing Cycle. *Buildings* **2023**, *13*, 1522. https://doi.org/10.3390/buildings13061522

Academic Editors: Cong Ma, Chenggao Li, Haijun Zhou, Rujin Ma and Rui Zhou

Received: 19 April 2023
Revised: 15 May 2023
Accepted: 5 June 2023
Published: 13 June 2023

1. Introduction

Under complex conditions such as extreme cold and high altitude and various problems such as leakage, block falling and collapse can occur during the operation of transportation infrastructure [1,2], which poses a significant threat to the long-term service performance of tunnel structure and the safety of vehicle operation.

When a structure is affected by disease, commonly used reinforcement methods include secondary pouring concrete, external prestressing, double liquid grouting, and pasting FRP [3–8]. However, these methods are often time-consuming, labor-intensive, and costly. In contrast, Engineered Cementitious Composite (ECC) [9–11] has excellent crack control ability [12,13], high toughness, and impact resistance [14], and its ultimate failure strain can reach over 3% [15], exhibiting obvious strain hardening characteristics. ECC materials have a high elastic modulus [16], corrosion resistance [17], and frost resistance due to the internal fibers. As a result, some researchers have begun to use ECC materials in concrete reinforcement [18–21]. The results demonstrate that ECC not only improves the crack load and ultimate load of reinforced concrete beams but also disperses cracks, controls crack width, and limits crack development. The cracks in ECC-reinforced concrete beams are fine and dense, and the number of cracks is obviously larger than that of ordinary reinforced concrete beams. Qin et al. [22] used ECC material to reinforce seven types of concrete beams, and the test results showed that ECC effectively slowed down the crack development in the tensile zone of concrete beams, improving fracture ductility and energy absorption capacity. Furthermore, some scholars have used ECC as a matrix binder for FRP (plate or grid) to reinforce the beams. Yang et al. [23] conducted a series of experiments on the flexural behavior of RC beams strengthened with Carbon Fiber Reinforced Plastics (CFRP) and ECC, and the results showed that ECC was an ideal cementitious matrix for strengthening applications using FRP grids as external reinforcement. Hou et al. [24] investigated a reinforcement system made of basalt fiber reinforced polymer and ECC matrix to reinforce RC beams, and the results demonstrated that the reinforced beams could effectively improve the ultimate failure load by more than 30% compared to traditional concrete beams. Gao [25] studied ECC-high strength reinforced concrete composite beams and found that the bearing capacity of composite beams was higher than that of traditional concrete beams. Additionally, Ge [26] studied the flexural performance of TRC-concrete beams and found that replacing some concrete with ECC could not only improve the bearing capacity of the structure but also effectively enhance the ability of the members to resist cracking and deformation. Table 1 summarizes the conducted research upon ECC and ECC-NC systems.

Good interfacial bonding characteristics are the basis for the cooperative work between ECC and NC and are the key to delaying the damage of reinforced concrete structures and ensuring that steel bars do not corrode. Upon ECC-NC, domestic and foreign scholars have mainly focused on factors such as interfacial bonding mode, interfacial curing time, interfacial roughness, concrete strength grade, thickness of reinforcement layer, changes in ECC mix ratio, and temperature influences [27–33]. On this basis, a series of tests such as the ECC-NC bonding interface tensile strength test [34,35], shear test [36], and bending test [18] have been carried out. The test results have shown that these factors have an impact on the performance of the bonding interface and that the failure modes and crack propagation modes [37] of ECC are also different due to the different types of fibers in ECC [37,38]. In addition, some scholars have studied the damage behavior of the concrete–concrete interface under different ECC strength grades and interface roughness under salt freeze–thaw cycles [37,38]. Salt freeze–thaw cycles significantly reduce the interface bonding behavior and interface fracture performance. The interface strength is influenced to varying degrees with an increase in salt freezing grade. In terms of durability, Yin et al. [39,40] have research results which show that TRC reinforced concrete beams can better resist chloride attack in a chloride environment than unreinforced reinforced concrete beams. Although the bearing capacity of TRC reinforced beams decreases in chloride environment, the decrease is negligible compared with ordinary reinforced concrete beams.

Table 1. Summary of ECC and ECC-NC tests.

Concrete Substrate	Test Method	Reference	Studied Parameters
ECC	Tensile test Bending test Shear test	[10,14,16] [12,14,16,18] [16]	Type and strength of cement matrix materials, the type of fibers, effect of geometric type, and weaving method of PE added
ECC-NC	Tensile test Bending test Shear test	[31,32,34,35] [19–21,23,25–29,32] [32,36]	Interfacial failure mode, interfacial bonding strength, interface roughness, effects of concrete strength grade, thickness of reinforcement layer, changes in ECC mix ratio, and temperature

FRP often uses epoxy resin as the binder, which is prone to fracture in complex environments and cannot make FRP exert its ultimate bearing capacity. TRECC not only has good fracture ductility but also has good bonding performance with FRP. In the concrete reinforcement system, it can effectively control the cracks when the concrete is destroyed.

Thus, it presents multiple cracks and improves the ultimate bearing capacity. Using ECC as a bonding matrix material and FRP (grid cloth) for concrete reinforcement has gained attention from experts and scholars. Xu Shilang's team [41–46] has conducted a series of studies on TRC, including the tensile mechanical model of TRC, the flexural performance of TRC-reinforced concrete beams, crack resistance, bonding and lapping performance, and fatigue performance of flexural beams. Yin Shiping [47–50] of Xu Shilang's team also studied the axial compression performance, crack behavior, and normal section bearing capacity of TRC-reinforced concrete columns, as well as the effective methods to improve the anti-stripping ability of fiber woven mesh protective layer concrete. Xun Yong [20,51] proposed a method of using textile-reinforced concrete (TRC) thin plate to strengthen reinforced concrete beams and conducted an experimental study on the shear capacity of inclined section of RC beams reinforced with TRC. Liu Dejun et al. [52] proposed a whole process analysis method for the normal section stress of fiber woven mesh reinforced concrete reinforced tunnel lining and carried out a series of verification tests. A large number of experiments show that TRC is a very effective material for structural reinforcement and enhancement. Through the above experiments, it is found that the reasonable ratio of ECC and FRP can improve the mechanical properties and meet the needs of production and life.

Durability is the most critical aspect of high-performance concrete, and it is necessary to investigate its mechanical properties of high-performance concrete under freeze–thaw cycles. Sun W. [53] discussed the damage caused by load and freeze–thaw cycles on concrete and its dependence on different concrete strength grades and analyzed the inhibitory effect of aerated and steel fibers on damage. The study also measured the loss of dynamic elastic modulus and flexural strength of specimens subjected to freeze–thaw cycles. Experts and scholars have also conducted extensive research on the durability, life prediction [54,55], bending, and bending properties [56–59] of reinforced concrete under freeze–thaw cycles. In addition, Murali G. et al. [60] tested and analyzed the impact failure strength of steel–concrete fiber reinforced concrete under freeze–thaw cycles.

In summary, although many scholars have conducted extensive research on TRECC and TRECC-NC, few studies on TRECC reinforced NC structures in cold regions have been carried out. To investigate the reinforcement mechanism of the repair system composed of TRECC and TRECC-NC under the influence of freeze–thaw cycles, this paper studies the tensile and flexural properties of TRECC and TRECC-NC specimens with varying roughness under 0–300 freeze–thaw cycles. In addition, in order to better understand the micro-level enhancement mechanism of TRECC under freeze–thaw cycles, SEM scanning electron microscopy and electron microscopy are used to observe freeze–thaw damage at the interface of TRECC1-NC and inside ECC. This paper is organized as follows: Section 2 describes the preparation of raw materials and adhesive systems. Section 3 outlines the test procedures and test methods. The test results and discussion are presented in Section 4, and the Section 5 provides the main conclusions of this paper.

2. Materials and Methods

2.1. Materials

In this study, P.O 42.5 ordinary Portland cement with a relative density of 3.14 g/cm^3 and a standard consistency water consumption of 25.9% was used. The chemical composition of the cement is shown in Table 2. Grade I fly ash with a fineness of 6.5% (sieve size 45 μm) and a water demand ratio of 96.8% was used, with a silicon dioxide content of 96.2%. Fine quartz sand was used as the fine aggregate, with particle size ranging from approximately 0.15 mm to 0.32 mm. The water reducer used was PCA-I, a polycarboxylate superplasticizer with a water reduction rate of 30%. The PE fiber and two types of FRP grid cloth (see Figure 1) are listed in Table 3.

Table 2. Technical parameters of P.O 42.5 cement.

Standard Consistency Water Consumption/%	Initial Setting Time/min	Final Setting Time/min	Burning Rate/%	MgO/%	SO_3/%	Cl^-/%	Stability
25.9	165	220	3.5	2.18	1.93	0.009	qualified

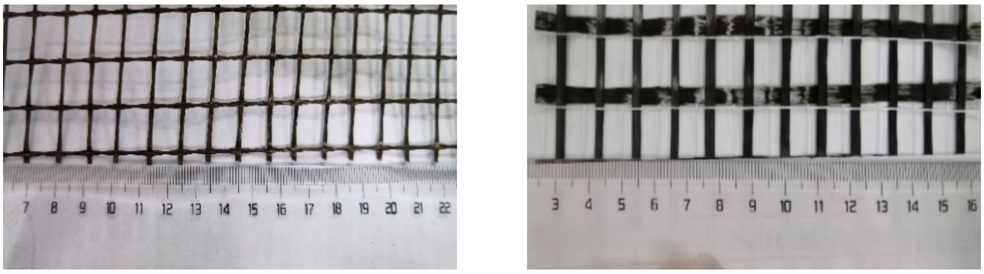

(**a**) (**b**)

Figure 1. Diagram of FRP gridding cloth. (**a**) BFRP gridding cloth; (**b**) CFRP gridding cloth.

Table 3. Mechanical properties of fibers.

Name	Density/(g/cm)	Tensile Strength/MPa	Elastic Modulus/GPa	Maximum Elongation/%	Diameter/μm	Length/mm	Mesh Width/mm
PE fiber	0.97	2900	116	2.42	31	12	-
BFRP gridding cloth	1.9	1700	80	2.16	-	-	10
CFRP gridding cloth	1.8	3400	240	1.6	-	-	10

2.2. Sample Preparation

The TRECC reinforcement system studied in this paper is mainly divided into two types of tests, i and ii, as shown in Figure 2. Each type of test piece has to undergo 0–300 freeze–thaw cycles, a total of 288 test pieces. Each type of test piece is tested three times, and the test results are taken as the average of three experiments.

(i) Mechanical properties test of TRECC under freeze–thaw cycles

The type i test comprises a uniaxial tensile test and three-point bending test. The uniaxial tensile specimens are categorized into three groups: TRECC, B-TRECC0, and C-TRECC0. The thickness of the uniaxial tensile specimen is 50 mm. To simulate the concrete protective layer's thickness in real reinforcement environment, the specimens containing FRP are poured with a total of 3 layers of FRP (BFRP or CFRP) every 17.5 mm. The three-point bending specimens are also classified into three types: TRECC, B-TRECC0, and C-TRECC0, with a total thickness is 40 mm and an interval of 17.5 mm between each layer. Two layers of FRP (BFRP or CFRP) are laid in these specimens.

(ii) Mechanical properties test of TRECC1-NC under freeze–thaw cycles

For the type ii reinforcement and repair system specimens, the uniaxial tensile specimens are composed of TRECC and NC. The three-point bending specimen is composed of ECC, NC, and FRP (BFRP and CFRP). In order to avoid the neutral axis effect, the NC layer is 30 mm and the ECC layer is 10 mm (including two types of FRP mesh).

The bonding interface between ECC and NC is shown in Figure 2a–c, and the average vertical height difference is used to quantitatively evaluate the interface roughness. The pouring process of uniaxial tensile specimens and three-point bending tensile specimens is shown in Figure 2d,e. The basic mixing ratio of NC and TRECC is shown in Table 4. The mixing time of ECC layer and NC layer is about 15 min and 5 min, respectively. The specimen naming rules are shown in Table 5, and the interface roughness is shown in Table 6.

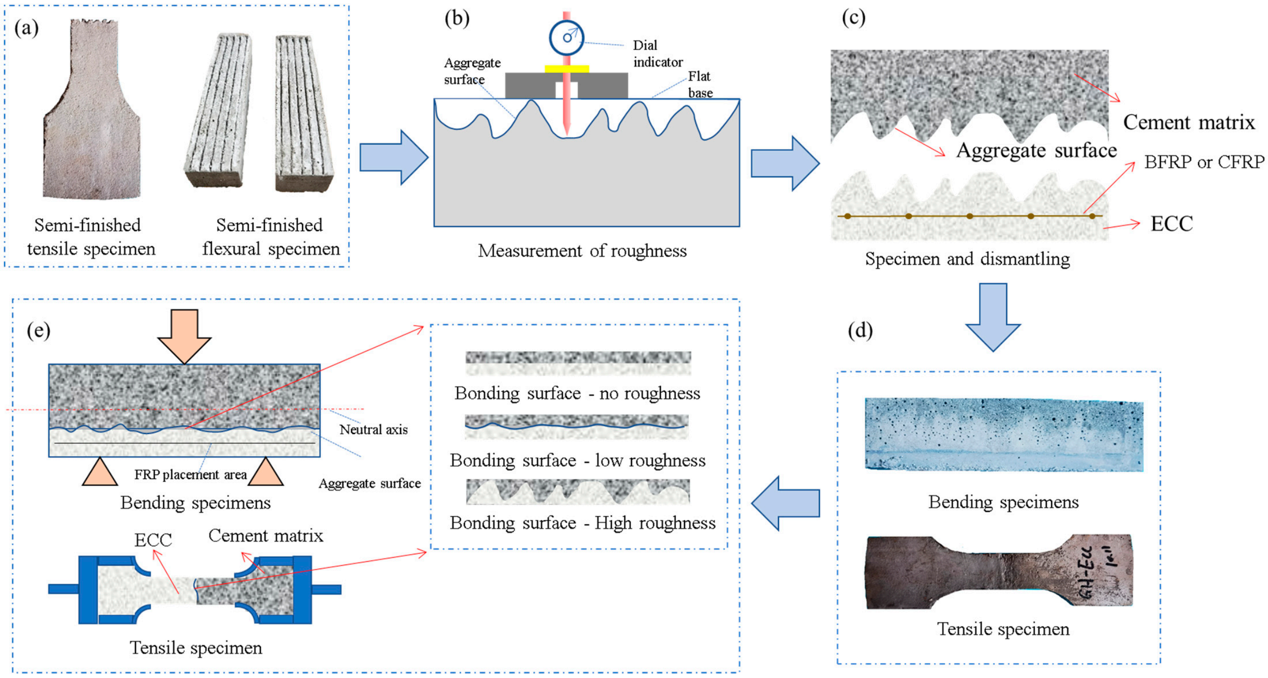

Figure 2. Analysis of bonding interface: (**a**) creating the roughness; (**b**) measuring the roughness; (**c**) diagram of the interface between two materials; (**d**) preparing specimens; (**e**) bending and tensile tests.

Table 4. Basic mix proportion of materials (kg/m^3).

Materials	Cement	Silica Fume	Fly Ash	Quartz Sand	Water Reducing Admixture	Water Cement Ratio	Fiber Content
PE-ECC	390	50	850	460	6	0.24	2%
Cement matrix	500	-	-	1500	0.6	0.4	-

Table 5. Naming rule of test specimen.

	TRECC		TRECC-NC	
	Uniaxial Tension	**Three-Point Bending**	**Uniaxial Tension**	**Three-Point Bending**
No FRP	TRECC0	TRECC1	TRECC0-NC	TRECC1-NC
BFRP	B-TRECC0	B-TRECC1	B-TRECC0-NC	B-TRECC1-NC
CFRP	C-TRECC0	C-TRECC1	C-TRECC0-NC	C-TRECC1-NC

Table 6. Key components of TRECC layer for each repaired system group.

Specimen Name	Bending Specimen Roughness	Tensile Specimen Roughness	Type of FRP	PE Fiber (%)	Freeze–Thaw Times/Times
0	-	-	-	-	0~300
No roughness	0	0	-	2	0~300
Low roughness	0.104	0.056	BFRP	2	0~300
High roughness	0.247	0.103	CFRP	2	0~300

3. Experimental Program and Methods

The research ideas of this paper are shown in Figure 3. The test is divided into three parts: 1, 2, and 3. The main test methods for the influence of freeze–thaw cycles on TRECC and TRECC-NC materials include:

1. After 24 h of casting, the sample was removed and placed in a standard curing chamber with a temperature of 20 °C ± 2 °C and humidity of ≥95% [61]. One week before the freeze–thaw test, the specimens required in the two types of tests i and ii were taken out and dehumidified at room temperature, and the specimens were placed in a rapid freeze–thaw test box. According to the "ordinary concrete long-term performance and durability test method" (GB/T50082-2009) [62], the rapid freeze–thaw method requires that each freeze–thaw cycle should be 6 h, and the melting time should not be less than 1/4 of the freezing time. During freezing and thawing, the center temperature of the specimen should be controlled at −18 °C ± 2 °C and 5 °C ± 2 °C, respectively. Therefore, the test temperature is −18 °C; the freezing time is 4 h, and the melting time is 2 h.
2. The mechanical properties test and microstructure test were carried out. The following tests were carried out on the i and ii specimens:
   (1) Tensile test: SANS electronic universal testing machine, loading rate of 0.2 mm/min [63,64], tensile way perpendicular to the bonding surface.
   (2) Bending test: The three-point bending test was carried out using an electronic universal testing machine controlled by SANS (Bairoe, Shanghai, China). The loading rate was 0.1 mm/min, and the load–displacement curve was automatically recorded in the bending test.
   (3) Microstructure analysis: Zeiss Sigma 300, Oberkochen, Germany, (magnification 10–106 times) was used for the TRECC reinforcement layer after freeze–thaw cycles; acceleration voltage: 0.02–30 kV) SEM electron microscope test; the bonding interface between TRECC-NC was observed using an electron microscope.
3. The mechanical properties and microscopic phenomena of the TRECC and TRECC-NC repair system under different roughness under 0–300 freeze–thaw cycles were analyzed.

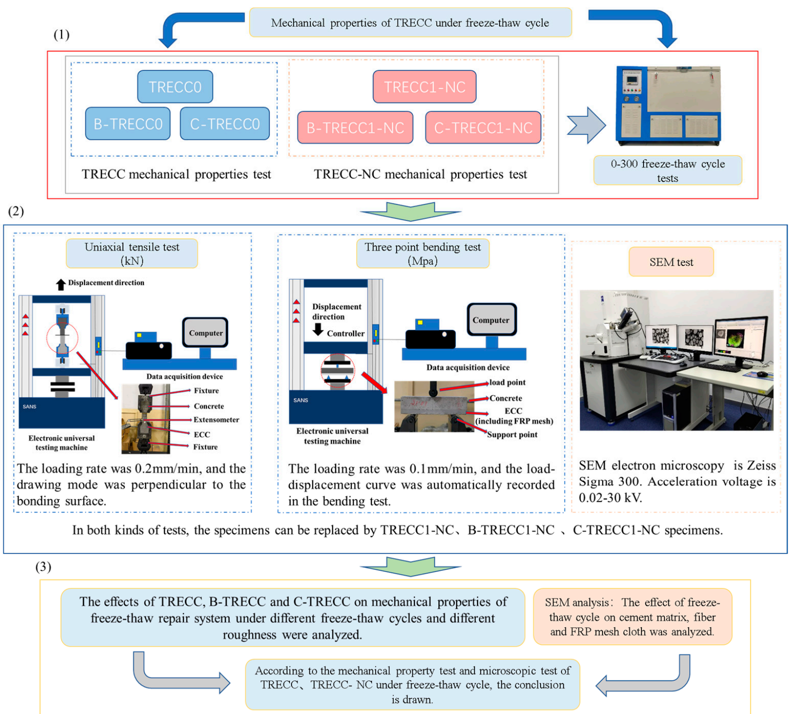

Figure 3. Workflow of the article: (**1**) overall testing specimens; (**2**) detailed information of tests; (**3**) analysis content.

4. Results and Discussion

4.1. Mechanical Properties of TRECC Matrix Material under Freeze–Thaw Cycles

4.1.1. Tensile Test

Figure 4 shows the stress–strain curves of TRECC0, B-TRECC0, and C-TRECC0 specimens under different freeze–thaw cycles.

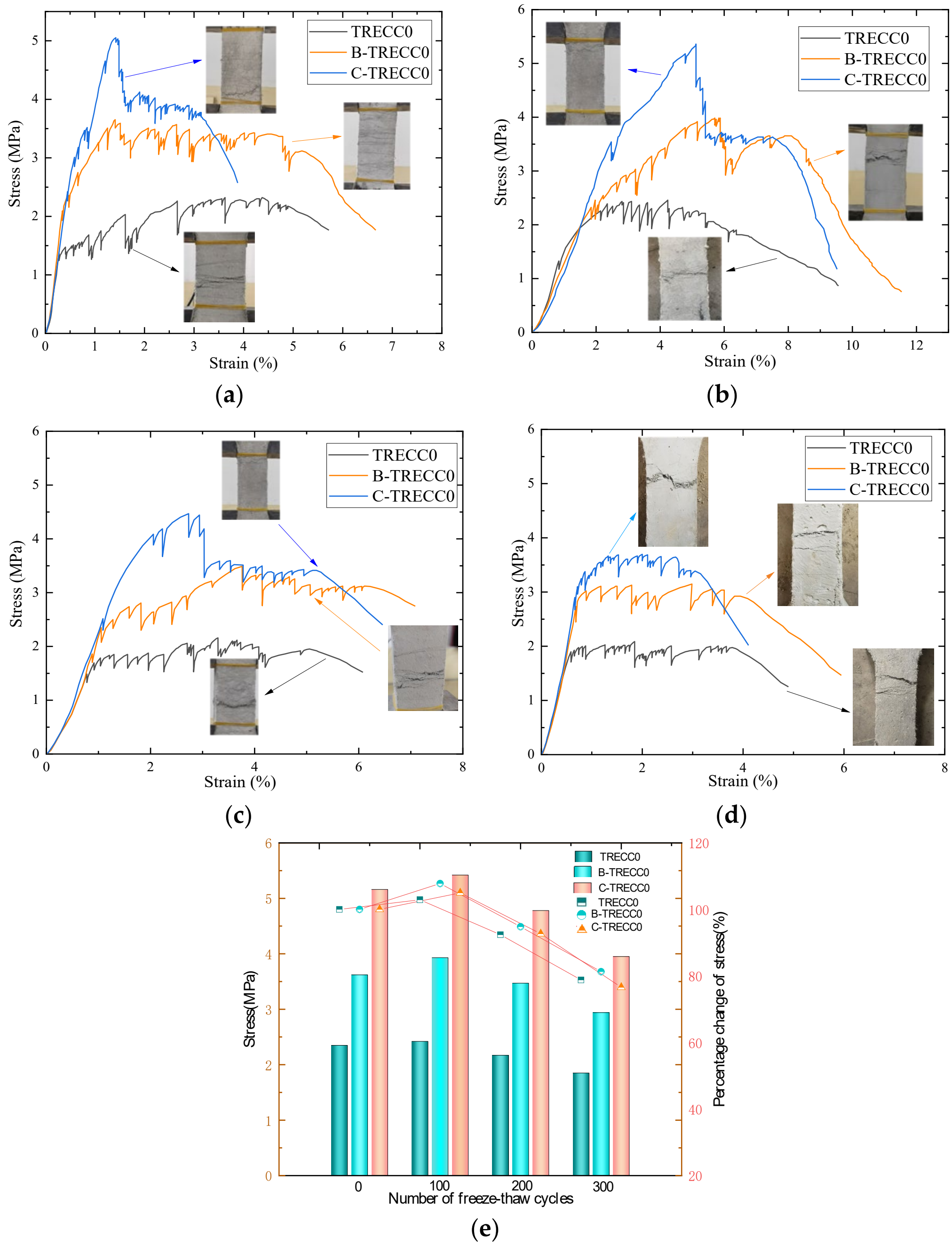

Figure 4. Experimental curve and comparison of uniaxial tensile properties under freezing–thawing cycles. (**a**) Zero freeze–thaw cycles; (**b**) 100 freeze–thaw cycles; (**c**) 200 freeze–thaw cycles; (**d**) 300 freeze–thaw cycles; (**e**) Variation of ultimate tensile strength under freeze–thaw cycles.

The mechanical properties of TRECC0 are not only related to the type and strength of cement matrix materials but also depend on various factors such as the type, geometric type, and weaving method of the added FRP. Figure 4a–e show that TRECC0, B-TRECC0, and C-TRECC0 specimens exhibit typical strain hardening characteristics under the action of 0–300 freeze–thaw cycles, and the strength is obviously improved with the addition of FRP grid cloth.

In the case of the TRECC0 specimen, the water–cement ratio of the specimen is small, and the internal structure is dense. With an increase of in the number of freeze–thaw cycles, the hydration reaction occurs inside the TRECC, and the fly ash begins to consume calcium hydroxide. For the TRECC0 specimen, the water–cement ratio of the specimen is small, and the internal structure is relatively dense. With the increasing number of freeze–thaw cycles, the hydration reaction occurs inside the TRECC, releasing hydration heat and reflecting heat release efficiency and the heat release process [63,64]. It shows that the fly ash in TRECC begins to consume calcium hydroxide [63,64], and hydrated calcium silicate is formed to fill the gel pores, capillary pores or voids, which reduces the weakening effect caused by the internal defects of the specimen [65,66]. After 100 freeze–thaw cycles, the tensile strength of the specimen increases by 2.9%.

The PE fibers in the TRECC specimen are distributed in multiple directions, creating voids during the pouring process. From Figure 5, it can be seen that the PE fibers in the TRECC sample are multiply distributed. Although secondary hydration reaction can fill some of these voids, it cannot compensate for all the defects. When subjected to freeze–thaw damage, the volume of PE fiber adsorbed water or the original water in the void increases after freezing, resulting in the cracking of the TRECC matrix material. After 300 freeze–thaw cycles, the ultimate tensile strength decreases by 22% compared to specimens subjected to 0 freeze–thaw cycles. For specimens containing TRECC (BFRP and CFRP), the bonding strength between FRP and the cement base is mainly divided into three parts: friction between the cement base and FRP preparation beam and the chemical glue force, followed by the tensile force formed by the heterotrophic distribution of PE in ECC through the grid cloth. As a result, the ultimate tensile strength of B-TRECC0 and C-TRECC0 increases by 33.6% and 53.8%, respectively, compared with 0 freeze–thaw cycles.

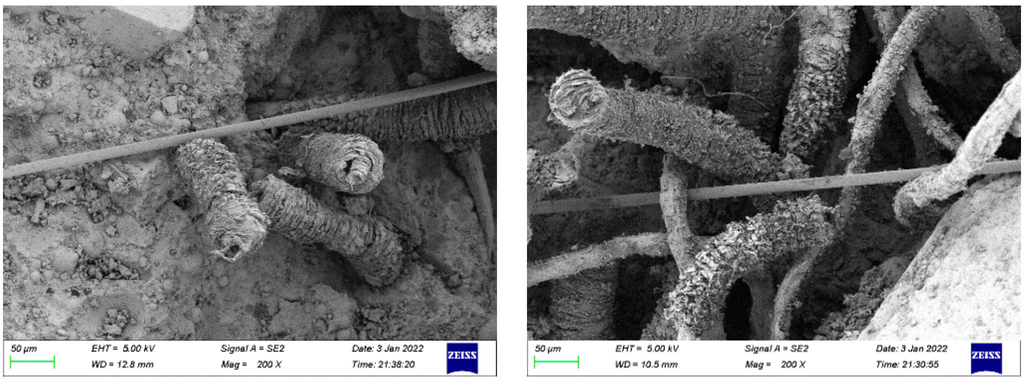

Figure 5. Multiple distribution of PE fiber.

With the increase of the number of freeze–thaw cycles, the secondary hydration reaction enhances the strength of the TRECC matrix and the mechanical bite force between the TRECC matrix and the FRP grid cloth, reaching its maximum value at 100 freeze–thaw cycles. The ultimate tensile strength of B-TRECC0 and C-TRECC0 increases by 38.4% and 55.3%, respectively, compared to TRECC. However, with the continuous accumulation of freeze–thaw damage, the internal cracks develop in the ECC matrix material, reducing the bridging force between the fibers and the matrix and the friction force between the FRP grid cloth and the concrete matrix. The ultimate tensile strength of the specimen is 5.2% and 7.3% lower than that of the 0 freeze–thaw cycle specimen. In comparison to TRECC specimens under 0 freeze–thaw cycles, the ultimate tensile strength of B-TRECC0 and C-TRECC0 increases by 32.2% and 50.8%. After 300 freeze–thaw cycles, the strength loss of TRECC matrix material offsets the bridging force caused by some PE fibers, resulting in a decrease in the ultimate strength of the specimens by 18.7% and 23.4%, respectively, compared to 0 freeze–thaw cycles but an increase of 20.06% and 40.5% compared to 300 freeze–thaw cycles.

In summary, the mechanical properties of the specimens are largely influenced by the geometry of FRP, the type of braiding, and the performance of the fiber monofilament. The complex fiber monofilament arrangement provides superior anchoring effect and positively affects the strength of TRECC. Under 0–300 freeze–thaw cycles, the ultimate bearing capacity of the three types of ECC specimens shows a trend of increasing first and then decreasing, and strain hardening occurred. The addition of FRP grid cloth leads to an increase in the strength of B-TRECC0 and C-TRECC0 compared with TRECC material. Due to the high ultimate tensile strength and elastic modulus of CFRP, C-TRECC0 outperforms B-TRECC0 in 0–300 freeze–thaw cycle tests, with the overall performance is C-TRECC0 > B-TRECC0 > TRECC0.

4.1.2. Bending Test

Figure 6 shows the load-deflection curves of TRECC, B-TRECC1, and C-TRECC1 flexural specimens under 0–300 freeze–thaw cycles.

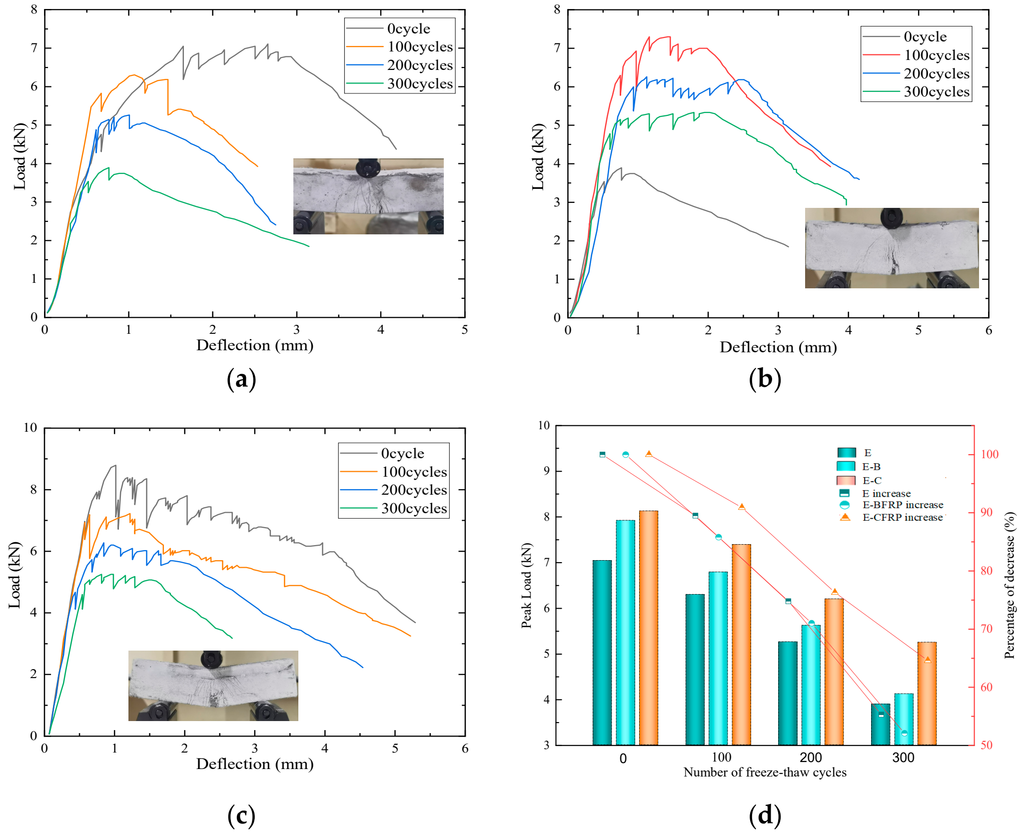

Figure 6. Load–deflection curve and comparison of the three-point bending test. (**a**) TRECC specimen; (**b**) B-TRECC1 specimen; (**c**) C-TRECC1 specimen; (**d**) ultimate bearing capacities of different specimens under freeze-thaw cycles.

From Figure 6, it can be seen that for TRECC1 specimens, the three-point bending test is carried out after 28 days of constant temperature curing. Each type of specimen is tested three times, and the test results are averaged. When the load increases to about 3.5 kN, the first crack appears in the specimen. With the progress of the freeze–thaw test, hydration reaction occurs inside the specimen. Fly ash interacts with calcium hydroxide precipitated from C_3S hydration and rapidly hydrates to form flocculent C-S-H gel. Hydration products with different particle sizes overlap and interweave with each other, plugging the defects such as cracks and voids inside the specimen. The secondary hydration reaction occurred inside the specimen, plugging the defects such as cracks and voids inside the specimen. However, the freeze–thaw damage offsets the enhancement effect caused by the secondary hydration reaction of fly ash. Compared with the 0 freeze–thaw TRECC1 specimen, the ultimate strength of the specimen decreased by 10.5%, 25.2%, and 44.7%, respectively, after 100, 200, and 300 freeze–thaw cycles. For the B-TRECC1 specimen, compared with 0 freeze–thaw cycles, after 100, 200, and 300 cycles of freeze–thaw damage, it decreases by 11.3%, 22.9%, and 43.4%, respectively. For C-TRECC1 specimens, compared with 0 freeze–thaw cycles, the damage of 100, 200, and 300 freeze–thaw cycles decreases by 17.2%, 28.2%, and 39.7%, respectively.

Due to the different production process of FRP, the bonding performance between FRP and the cement matrix will also be different. When subjected to bending load, FRP in TRECC specimens mainly exhibits tensile failure. Therefore, TRECC with CFRP shows higher mechanical properties than CFRP grid cloth. The reasons for this are as follows:

Without freeze–thaw cycles, the ultimate load of B-TRECC1 and C-TRECC1 specimens increases by 11.2% and 13.4%, respectively, compared with TRECC1 specimens. After 100 freeze–thaw cycles, the ultimate load of B-TRECC1 and C-TRECC1 specimens increases by 7.2% and 14.9%, respectively, compared with that of TRECC1 specimens under 0 freeze–thaw cycles. After 200 freeze–thaw cycles, the ultimate load of B-TRECC1 and C-TRECC1 specimens increases by 6.4% and 15.1%, respectively, compared with that of TRECC1 specimens under 0 freeze–thaw cycles. However, it decreases to the lowest after 300 freeze–thaw cycles, with an increase of 5.5% and 25.9%, respectively, compared with TRECC1 specimens under 0 freeze–thaw cycles.

4.2. Performance Test of TRECC-NC Repair System

4.2.1. Bending Test Results

As shown in Figure 6, with an increase in the number of freeze–thaw cycles, TRECC1-NC changes to a certain extent. After 0–150 freeze–thaw cycles, TRECC1-NC without roughness experiences debonding after being subjected to external load. After 150–300 freeze–thaw cycles, the specimen appears debonding at the bonding interface. Due to the existence of roughness, the development of cracks is limited, and the failure modes include a single crack along the load direction and multiple cracks along the load direction. The test results of bond strength and residual percentage of TRECC1-NC under freeze–thaw cycles are shown in Table 7. In order to consider the influence of different freeze–thaw cycles and different roughness on the mechanical properties of the TRECC1-NC repair system, the data are analyzed according to the results of three-point bending test, as shown in Figure 7.

Table 7. Three-point bending test results under different roughness and different freeze–thaw cycles.

Freeze–Thaw Cycles	Influencing Factor	Peak Load without Roughness/kN	Peak Load under Low Roughness/kN	Peak Load under High Roughness/kN
0 cycle	TRECC1-NC	2.81	3.42	3.92
	B-TRECC1-NC	3.69	4.36	5.36
	C-TRECC1-NC	4.01	5.12	6.01
100 cycles	TRECC1-NC	2.96	3.74	4.02
	B-TRECC1-NC	3.76	4.51	5.51
	C-TRECC1-NC	4.11	5.6	6.19
200 cycles	TRECC1-NC	2.21	3.01	3.52
	B-TRECC1-NC	2.96	3.82	4.98
	C-TRECC1-NC	3.26	4.73	5.36
300 cycles	TRECC1-NC	1.21	2.03	2.51
	B-TRECC1-NC	1.66	2.53	3.42
	C-TRECC1-NC	1.98	3.36	3.97

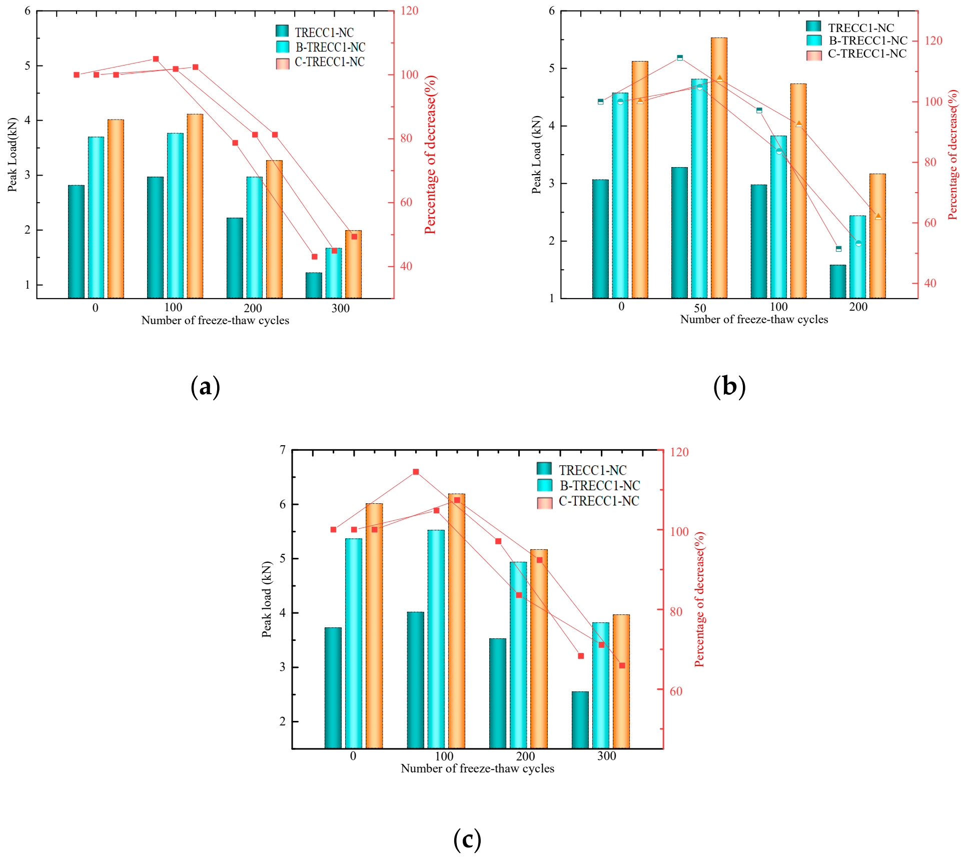

Figure 7. Peak load of TRECC-NC specimen with different roughness. (**a**) Roughness free; (**b**) Low roughness; (**c**) High roughness.

It can be seen from Table 7 and Figure 7 that compared with the three types of TRECC1-NC specimens without roughness under 0 freeze–thaw cycles, the ultimate bearing capacity of TRECC1-NC, B-TRECC1-NC, and C-TRECC1-NC increases by 23.8% and 29.9%, respectively, at 0 freeze–thaw cycles, with the peak load reaching its highest point at 100 freeze–thaw cycles, increasing by 25.2% and 31.6%, respectively. With the increase of the number of freeze–thaw cycles, freeze–thaw damage accumulates gradually in specimens without interface roughness, resulting in the loading capacity of the specimens decreasing by 21.3%, 19.7%, and 18.7%, respectively, compared to 0 times after 200 freeze–thaw cycles and decreasing by 56.9%, 40.9%, and 29.5%, respectively, after 300 freeze–thaw cycles.

For the three types of specimens of TRECC1-NC, B-TRECC1-NC, and C-TRECC1-NC with low roughness, the mechanical force between the interfaces offsets part of the load when the specimens are subjected to load due to the existence of the roughness. Under 100 freeze–thaw cycles, the ultimate loads of TRECC1-NC, B-TRECC1-NC, and C-TRECC1-NC increase by 6.4%, 4.9%, and 7.4%, respectively, compared to those under 0 freeze–thaw cycles. However, with the increase in freeze–thaw cycles, the bonding interface is continuously damaged, and the micro-cracks inside the specimen also continue to develop, causing the strength of the specimen to decrease. After 300 freeze–thaw cycles, the capacity reached its lowest point. Compared to 0 freeze–thaw cycles, the peak load decreased by 48.6%, 46.7%, and 38.2%, respectively.

When the bonding interface of TRECC1-NC, B-TRECC1-NC, and C-TRECC1-NC has high roughness, the cement paste of ECC undergoes hydration and hardening, creating a transition zone on the surface of NC. The existence of the transition zone enhances the performance of the specimen. When subjected to 0 freeze–thaw cycles, the ultimate load of the specimen improves by 26.8% and 34.7%, respectively. After the secondary hydration reaction, the ultimate load of the specimen subjected to 100 freeze–thaw cycles increases by 28.9% and 36.6%, respectively. However, with the continuous action of freeze–thaw cycles, the damage of the interface between the two continues to accumulate, and several small cracks at the cross section continue to expand, reducing the interface bonding strength. After 300 freeze–thaw cycles, the peak load of the specimens decreases by 2.3% and 6.1%, respectively.

4.2.2. TRECC0-NC Research on Interface Properties

Figure 8 shows the changes of tensile strength and ultimate tensile strain of TRECC0-NC material after 0, 100, 200, and 300 freeze–thaw cycles. As shown in Figure 8a, the chemical reaction of cement paste on the surface of TRECC0-NC results in the formation of a weak transition zone at the interface. During repair, a water film is formed on the surface of the old concrete, leading to a higher local water–cement ratio of the new concrete at the bonding surface than the water–cement ratio of the system. This, in turn, increases the porosity at the bonding interface and reduces the interface strength. After reaching the ultimate load, the rebound of the strength curve exhibits a small rebound, and there is no obvious strain-hardening characteristic. After 0 freeze–thaw cycles, the ultimate bearing capacity is 1.49 MPa. With an increase in the number of freeze–thaw cycles, the ultimate bearing capacity of the specimen initially increases first and then decreases. The ultimate bearing capacity of the specimen reaches the maximum value of 1.6 MPa under 100 freeze–thaw cycles. After 100 freeze–thaw cycles, it begins to decline, and after 300 cycles it will reach the minimum of 0.54 MPa.

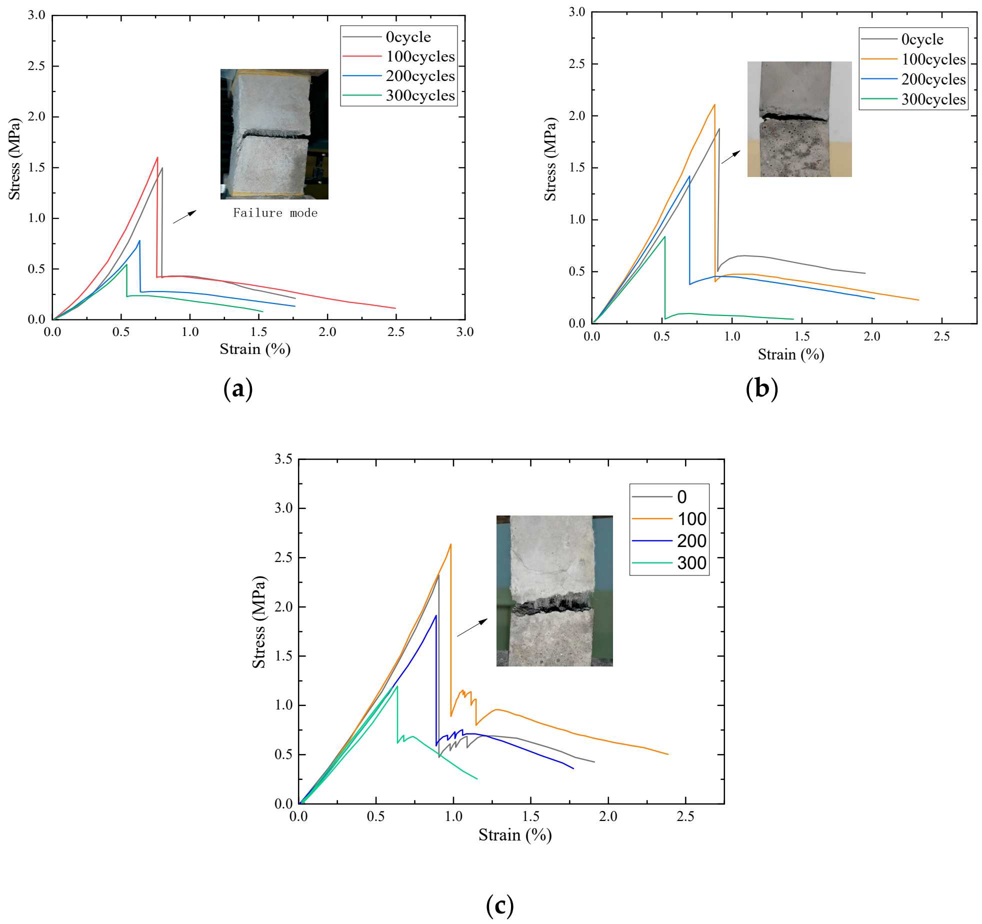

Figure 8. Stress–strain curve with different roughness. (**a**) No roughness TRECC0-NC; (**b**) Low roughness TRECC0-NC; (**c**) High roughness TRECC0-NC.

For TRECC0-NC specimens with low roughness, as shown in Figure 8b, due to the existence of the roughness of the bonding surface, there is a slight 'mechanical force' phenomenon between ECC and concrete. Under tensile load, the stress–strain curve rebounds after cracking, and strain-hardening characteristics begin to appear. Under the action of 0 freeze–thaw cycles, the ultimate bearing capacity of the specimen is 1.87 MPa. With an increase in the number of freeze–thaw cycles, the cement matrix of the bonding surface undergoes a secondary hydration reaction. After 100 freeze–thaw cycles, the dynamic capacity damage of the concrete matrix material begins to accumulate, and the ultimate bearing capacity of the specimen is 2.12 MPa. After 300 freeze–thaw cycles, the ultimate bearing capacity of the specimen decreased to a minimum of 0.72 MPa. Figure 8c shows that the TRECC0-NC specimen with high roughness shows good integrity between ECC and concrete under tensile load. The bond surface remains intact when the specimen is destroyed, and damage occurs inside the concrete. The uneven bond surface increases the contact area, and the exposed concrete aggregate and the uneven interface enhance the embedding effect between ECC and concrete. Due to the compactness of ECC, it effectively fills the voids and gaps of the bond surface and enhances the bond strength. After 0 freeze–thaw cycles, the ultimate bearing capacity of the specimen is 2.4 MPa. After 50 freeze–thaw cycles, the secondary hydration reaction of fly ash occurs, and the ultimate bearing capacity of the specimen is 3.21 MPa. After 100 freeze–thaw cycles, the freeze–thaw damage inside the concrete continues to accumulate, and the ultimate tensile strength is 2.68 MPa. After 300 freeze–thaw cycles, the ultimate bearing capacity of the specimen is 0.97 MPa.

The test results of bond strength and enhancement percentage of the TRECC0-NC repair system under freeze–thaw cycles are shown in Figure 9. For the three cases of no roughness, low roughness, and high roughness, it can be observed that regardless of whether the specimen undergoes freeze–thaw, the roughness between the bonding surfaces can effectively improve the bond strength. The bonding performance of the reinforcement system under high roughness is the best. The improvement of this performance mainly comes from the mechanical interlocking at the interface and the limiting effect of fiber in ECC on the dry shrinkage deformation and shrinkage deformation of cement matrix materials. After 50 freeze–thaw cycles, the bonding strength of the system reaches the highest. Compared to the flat surface, the ultimate tensile strength of the TRECC0-NC reinforcement system (0 freeze–thaw cycles) under low roughness and high roughness increases by 50.05% and 61.25%, respectively. After 50 freeze–thaw cycles, the ultimate tensile strength of the TRECC0-NC reinforcement system under low roughness and high roughness increases by 51.6% and 62.3%, respectively. After 100 freeze–thaw cycles, the ultimate strength of the three types of reinforced specimens decreased. After 300 freeze–thaw cycles, the ultimate tensile strength of the specimens decreases by 62.1% and 59.5% compared to that under 0 freeze–thaw cycles. These results indicate that the change of roughness at the interface can effectively improve the bonding performance of the repair system under freeze–thaw action.

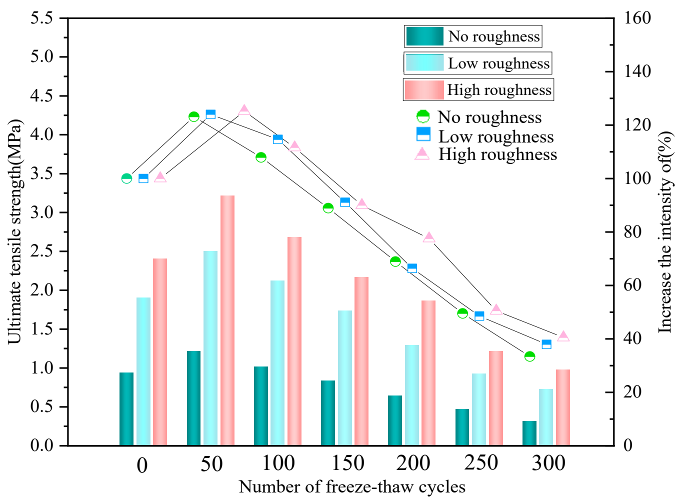

Figure 9. Stress increase of TRECC0-NC repair system.

4.3. Microstructural Analysis

Microscopic Observation

Figure 10 shows the electron microscope image of the TRECC1-NC bonding interface with plane roughness. The results indicate that the NC interface is affected by freeze–thaw cycles. As the presence of a water film results in a local water–cement ratio higher than the rest of the interface, excessive weak areas appear. Figure 10b displays a schematic diagram of TRECC1-NC failure with roughness in the bonding interface under saturated water conditions during the freeze–thaw cycle test. The osmotic pressure or hydrostatic pressure in the hole of the specimen causes periodic irreversible damage to the concrete matrix, which leads to the phenomenon of the concrete surface falling off and crisping. The existence of roughness can effectively improve the bonding area of TRECC1-NC, reduce the effect of an excessive weak area of the interface, and inhibit the erosion of freeze–thaw damage along the bonding surface.

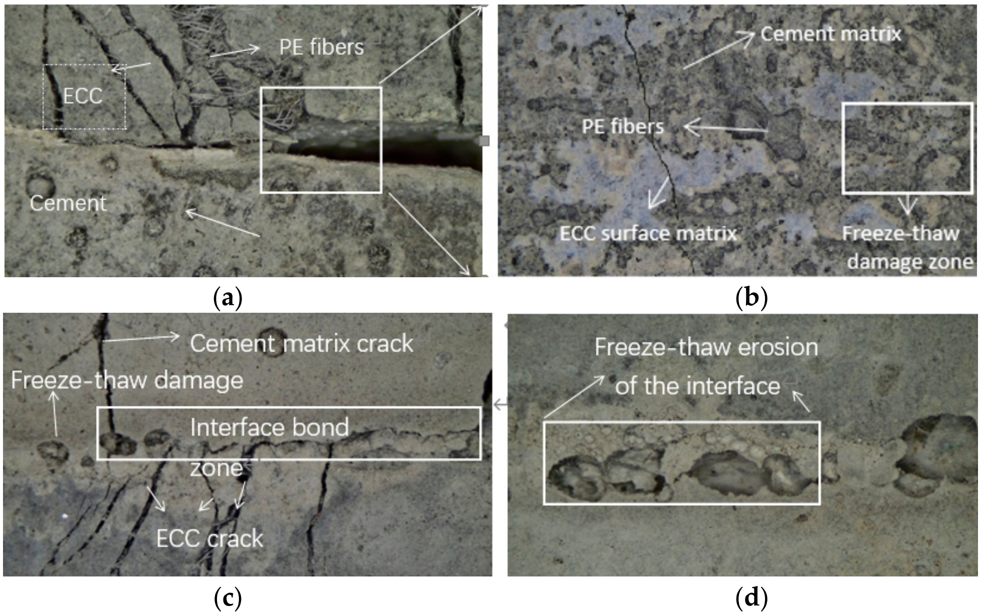

Figure 10. Diagram of bonding interface under different roughness. (**a**) No roughness; (**b**) Locally enlarged image; (**c**) Low roughness; (**d**) Locally enlarged image.

In order to further study the internal microstructure of the TRECC1-NC repair system under freeze–thaw cycles, SEM electron microscopy is employed to observe the typical failure modes. As shown in Figure 11a,b, the structure of hydration products of NC changes significantly under freeze–thaw cycles. NC is no longer a dense structure combined with gel and crystal but a loose structure interwoven with needles or rods, showing disorder. There are large pores in NC and bubbles in a completely closed state, and cracks gradually appear. After the fracture slip between the fiber and the cement-based material, a large quantity of the hydration products is still attached to the fiber (see Figure 11c). After the fiber is broken, dense cracks appear on it. Due to the test of the specimen in the saturated state, $Ca(OH)_2$ will be produced in the gap between the fiber and the cement base, which seriously reduces the bonding strength between the two. However, the pozzolanic activity of fly ash results in the production of hydration products that reduce the production of $Ca(OH)_2$ crystals and enhance the bonding between the fiber and the cement matrix [1]. As shown in Figure 11d, it can be observed that the FRP grid cloth has good bonding with the cement matrix, and the failure section of the FRP fiber bundle is broken, indicating that FRP plays a crucial role in the TRECC1-NC reinforcement system.

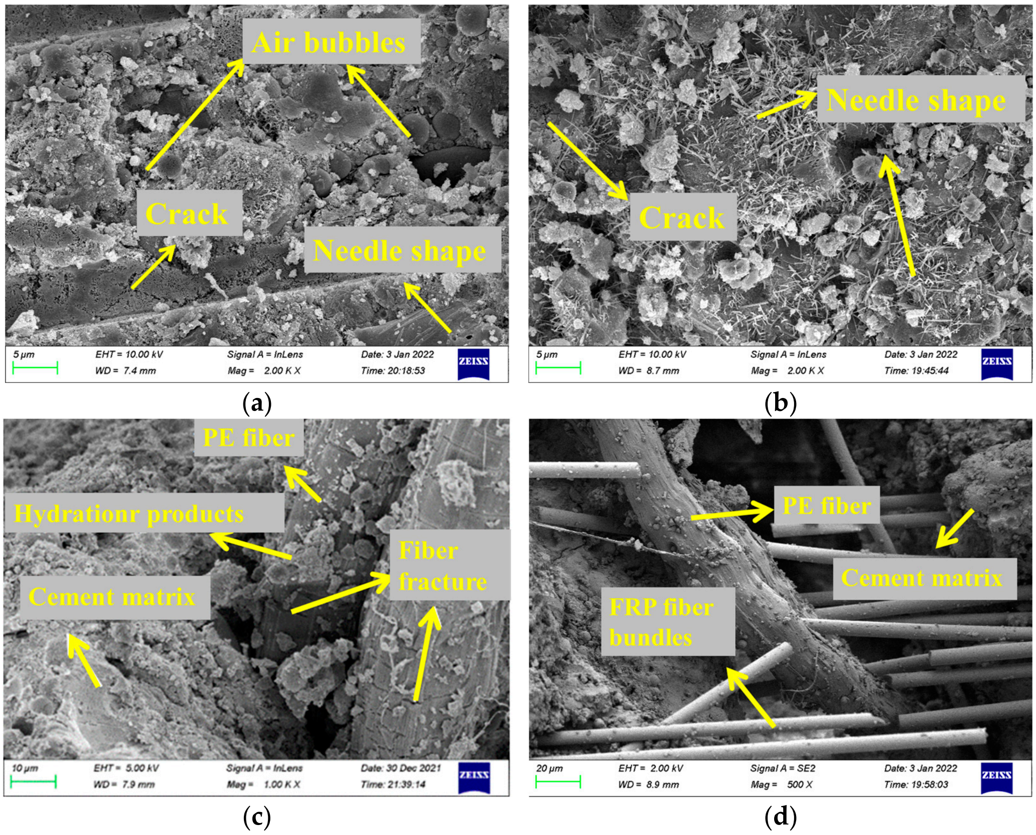

Figure 11. SEM electron microscopy. (**a**) SEM image of an early freeze–thaw cycle; (**b**) SEM image of a late freeze–thaw cycle; (**c**) SEM image of fiber-ECC interface after exposure to freeze–thaw damage; (**d**) SEM image of ECC and FRP subjected to freeze–thaw damage.

5. Conclusions

The study investigates the effects of different freeze–thaw cycles on the mechanical properties of ECC, ECC-FRP, and ECC-cement matrix repair systems with varying roughness and types of FRP grid cloth. The following conclusions are drawn from the test results:

1. In the tensile test of TRECC, B-TRECC, and C-TRECC, with the increase of the number of freeze–thaw cycles, the strength of the three types of specimens increases continuously. C-TRECC0 exhibits the best performance with an increase 55.3% for 100 freeze–thaw cycles and 50.8% for 200 freeze–thaw cycles compared to TRECC. However, after 300 freeze–thaw cycles, the ultimate strength of the specimen is reduced by 23.4%, compared to 0 freeze–thaw cycles.
2. For TRECC1-NC, B-TRECC1-NC, and C-TRECC1-NC specimens, adding FRP grid cloth or increasing interface roughness can effectively improve the strength of the specimens, whether at room temperature or under the action of freeze–thaw cycles. Due to the existence of roughness, the bite force and friction force between the bonding interface are increased from 0 to 300 freeze–thaw cycles. The mechanical properties with the highest roughness show the best mechanical performance. The reinforcement effect of FRP is as follows: BFRP > CFRP > ECC.
3. With the increase of freeze–thaw cycles, the mechanical performance of the TRECC0-NC repair system can be affected. The ultimate failure strength of the specimens with three degrees of roughness increases initially and then decreases with the accumulation of freeze–thaw cycles. Moreover, the bonding performance of the reinforcement system with the highest roughness shows the best.
4. The ECC-NC repair system was found to be susceptible to freeze–thaw damage, and the amount of surface spalling also showed a significant correlation with its flexural strength. ECC exhibits good cracking control ability, which increases with the interfa-

cial roughness and shows good frost resistance and secondary strengthening effect under freeze–thaw cycles. However, as the freeze–thaw cycle process continues, their cooperative working ability is weakened. Nevertheless, due to the dense compactness of ECC, the internal fiber of ECC and the concrete matrix exhibits good adhesion even after undergoing freeze–thaw cycles. It is found that the specimen can exhibit good strain-hardening characteristics when it begins to fracture.

5. This study can effectively solve the problems of time-consuming, cumbersome steps and expensive prices of traditional concrete reinforcement methods. Results indicate that using B-TRECC or C-TRECC can maximize the mechanical properties of FRP and limit the cracking process of concrete to a certain extent, which can be utilized to reinforce the cracking components or damaged engineering structures in cold regions.

Author Contributions: Conceptualization, F.X. and Q.L.; methodology, F.X.; software, Q.L.; validation, T.M., Y.Z. and T.B.; formal analysis, Q.L.; investigation, Q.L. and T.B.; resources, F.X.; data curation, T.M. and J.L.; writing—original draft preparation, Q.L. and T.M.; writing—review and editing, T.M., J.L. and Y.Z.; supervision, Y.Z.; project administration, F.X. All authors have read and agreed to the published version of the manuscript.

Funding: This research was funded by National Natural Science Foundation of China (grant number 52078311), Shenzhen Science and Technology program (grant number KQTD 20180412181337494), Natural Science Foundation of Hebei Province (grant number E2021210099), and Project of Science and Technology Research and Development Program of China Railway Corporation (grant number N2022G033).

Data Availability Statement: Data will be available on request.

Conflicts of Interest: The authors declare no conflict of interest.

References

1. Zheng, X.Y.; Wang, Y.; Zhang, S.Q.; Xu, F.; Zhu, X.; Jiang, X.; Zhou, L.; Shen, Y.; Chen, Q.; Yan, Z.; et al. Research progress of the thermophysical and mechanical properties of concrete subjected to freeze-thaw cycles. *Constr. Build. Mater.* **2022**, *330*, 127254. [CrossRef]
2. Jia, H.Y. Theoretical Model and Experimental Study on Freeze-Thaw Damage Mechanism of Porous Rock and Fractured Rock Mass. Ph.D. Thesis, China University of Geosciences, Xi'an, China, 2016.
3. Chen, J.X. Research on Prevention and Control Technology of Tunnel Frost Damage. Master's Thesis, Chang'an University, Xi'an, China, 2007.
4. Feng, Q.; Wang, G.; Jiang, B.S. An analytical method for the analysis of tunnel surrounding rock melting in seasonal cold regions. *J. Geotech. Eng.* **2015**, *37*, 1835–1843.
5. Luo, Y.B. Study on Frost Damage Classification and Prevention Technology of Tunnel in Cold Region. Ph.D. Thesis, Beijing Jiaotong University, Beijing, China, 2010.
6. Lai, Y.M.; Wu, Z.W.; Zhu, Y.L.; Ling, F.; Zhu, L.N. Viscoelastic analytical solution of frost heaving force of tunnel in cold region. *J. Railw.* **1999**, *6*, 70–74.
7. Wang, H.; Chen, W.Z. Sensitivity analysis of mechanical parameters of surrounding rock of Galongla tunnel to deformation. *J. Geotech. Eng.* **2012**, *34*, 1548–1553.
8. Lai, J.; Wang, X.; Qiu, J.; Zhang, G.; Chen, J.; Xie, Y.; Luo, Y. A state-of-the-art review of sustainable energy based freeze proof technology for cold-region tunnels in China. *Renew. Sustain. Energy Rev.* **2018**, *82*, 3554–3569. [CrossRef]
9. Li, M.; Li, V.C. High-early-strength ECC for rapid durable repair, material properties. *ACI Mater.* **2011**, *108*, 3–12.
10. Zhang, Z.; Qin, F.; Ma, H.; Xu, L. Tailoring an impact resistant engineered cementitious composite (ECC) by incorporation of crumb rubber. *Construct. Build. Mater.* **2020**, *262*, 120116. [CrossRef]
11. Li, M.; Li, V.C. Cracking and healing of engineered cementitious composites under chloride environment. *ACI Mater.* **2011**, *108*, 333–340.
12. Zhang, Z.G.; Hu, J.; Ma, H. Feasibility study of ECC with self-healing capacity applied on long-span steel bridge deck overlay. *Int. J. Pavement Eng.* **2019**, *20*, 884–893. [CrossRef]
13. Zhou, J.; Pan, J.; Leung, C.K. Mechanical behavior of fiber-reinforced engineered cementitious composites in uniaxial compression. *Mater. Civ. Eng.* **2015**, *27*, 04014111. [CrossRef]
14. Lin, Z. Research on Impact Resistance of ECC Crash Barrier Material. Master's Thesis, Southeast University, Nanjing, China, 2017.
15. Li, V.C.; Wu, C.; Wang, S.; Ogawa, A.; Saito, T. Interface tailoring for strain-hardening polyvinyl alcohol-engineered cementitious composite(PVA-ECC). *ACI Mater.* **2002**, *99*, 463–472.

16. Zhou, S.; Xie, L.; Jia, Y.; Wang, C. Review of Cementitious Composites Containing Polyethylene Fibers as Repairing Materials. *Polymers* **2020**, *12*, 2624. [CrossRef] [PubMed]
17. Zhang, Z.; Zhang, Q.; Li, V.C. Multiple-scale investigations on self-healing induced mechanical property recovery of ECC. *Cem. Concr. Compos.* **2019**, *103*, 293–302. [CrossRef]
18. Colombo, I.G.; Colombo, M.; Prisco, M.D. Bending behaviour of textile reinforced concrete sandwich beams. *Constr. Build. Mater.* **2015**, *95*, 675–685. [CrossRef]
19. Sheng, J.; Yin, S.P.; Wang, F.; Yang, Y. Experimental study on the fatigue behaviour of RC beams strengthened with TRC after sustained load corrosion. *Constr. Build. Mater.* **2017**, *131*, 713–720.
20. Xun, Y.; Zhi, Z.D.; Zhang, Q. Experimental research on flexural behavior of reinforced concrete beams strengthened with textile reinforced concrete sheets. *Build. Struct.* **2010**, *31*, 70–76.
21. D'Ambrisi, A.; Focacci, F. Flexural strengthening of RC beams with cement-based composites. *Compos. Constr.* **2012**, *15*, 707–720. [CrossRef]
22. Qin, F.J.; Zhang, Z.J.; Yin, Z.; Di, J.; Xu, L.; Xu, X. Use of high strength, high ductility engineered cementitious composites(ECC) to enhance the flexural performance of reinforced concrete beams. *J. Build. Eng.* **2020**, *32*, 101746. [CrossRef]
23. Yang, X.; Gao, W.Y.; Dai, J.-G.; Lu, Z.-D.; Yu, K.-Q. Flexural strengthening of RC beams with CFRP grid-reinforced ECC matrix. *Compos. Stuctures* **2018**, *189*, 9–26. [CrossRef]
24. Hou, W.; Li, Z.Q.; Gao, W.-Y.; Zheng, P.-D.; Guo, Z.-X. Flexural behavior of RC beams strengthened with BFRP bars-reinforced ECC matrix. *Compos. Stuctures* **2022**, *241*, 112092. [CrossRef]
25. Gao, S.L.; Guo, Y.D.; Wu, Y.Q. Experimental and theoretical study on flexural capacity of ECC / reinforced concrete composite beams. *Civ. Build. Environ. Eng.* **2017**, *39*, 123–131.
26. Ge, W.J.; Zong, Y.F.; Qiu, S.W.; Song, W.R.; Wang, Y.; Lu, W.G.; Cao, D.F.; Ashraf, A. Study on flexural behavior of BFRP bar-ECC-concrete composite beams strengthened with carbon fiber sheet. *J. Build. Struct.* **2021**, *42*, 302–311.
27. Yu, J.T.; Xu, W.L.; Zhang, Y.M. Experiment study on fracture property of ECC-concrete interface. *Build. Mater.* **2015**, *18*, 958–963.
28. Zhang, J.; Li, V.C. Monotonic and fatigue performance in bending of fiber-reinforced engineered cementitious composite in overlay system. *Cem. Concr. Res.* **2002**, *32*, 415–423. [CrossRef]
29. Liu, W.; Xu, S.; Li, Q. Flexural behaviour of UHTCC-layered concrete composite beam subjected to static and fatigue loads. *Fatigue Fract. Eng. Mater. Struct.* **2013**, *36*, 738–749. [CrossRef]
30. Bu, L.; Zhou, N.; Lu, C.; Li, W. Research on the bond-performance of polyvinyl alcoholengineered cementitious composite to concrete. *Shandong Univ. Eng. Sci.* **2012**, *42*, 45–51.
31. Wang, B.; Xu, S.; Liu, F. Evaluation of tensile bonding strength between UHTCC repair materials and concrete substrate. *Constr. Build. Mater.* **2016**, *112*, 595–606. [CrossRef]
32. Wang, N. Experimental Research on Bonding Mechanical Performance between Ultra High Toughness Cementitious Composites (UHTCC) and Existing Concrete. Ph.D. Thesis, Dalian University of Technology, Dalian, China, 2011.
33. Deng, Z.C.; Xue, H.Q. Experiment and study on direct shear behavior for adhesion of fiber reinforced high ductility cementitious composites on existing concrete. *Highw* **2011**, *2*, 027.
34. Gao, S.; Zhao, X.; Qiao, J.; Guo, Y.; Hu, G. Study on the bonding properties of Engineered Cementitious Composites(ECC) and existing concrete exposed to high temperature. *Constr. Build. Mater.* **2019**, *196*, 330–344. [CrossRef]
35. Hu, C.H. Research on the Interfacial Bonding Behavior of Existing Concrete Members Repaired with SHCC. Ph.D. Thesis, Xi'an University of Architecture and Technology, Xi'an, China, 2013.
36. Tian, J.; Wu, X.; Zheng, Y.; Hu, S.; Du, Y.; Wang, W.; Sun, C.; Zhang, L. Investigation of interface shear properties and mechanical model between ECC and concrete. *Constr. Build. Mater.* **2019**, *223*, 12–27. [CrossRef]
37. Wu, X.; Tian, J.; Ma, H.; Zheng, Y.; Hu, S.; Wang, W.; Du, Y.; Huang, W.; Sun, C.; Zhu, Z. Investigation on interface fracture properties and nonlinear fracture model between ECC and concrete subjected to salt freeze-thaw cycles. *Constr. Build. Mater.* **2020**, *259*, 119785. [CrossRef]
38. Tian, J.; Wu, X.; Zheng, Y.; Hu, S.; Ren, W.; Du, Y.; Wang, W.; Sun, C.; Ma, J.; Ye, Y. Investigation of damage behaviors of ECC-to-concrete interface and damage prediction model under salt freeze-thaw cycles. *Constr. Build. Mater.* **2019**, *226*, 238–249. [CrossRef]
39. Yin, S.P.; Yu, Y.; Xi, Y. Flexural performance of TRC-strengthened RC beam under chloride environment. *Anti-Corros. Methods Mater.* **2018**, *65*, 444–450.
40. Yin, S.P.; Yu, Y.; Na, M. Flexural properties of load-holding reinforced concrete beams strengthened with textile-reinforced concrete under a chloride dry-wet cycle. *Eng. Fibers Fabr.* **2019**, *14*, 1–9. [CrossRef]
41. Xu, S.L.; Yin, S.P.; Cai, X.H. Study on flexural behavior of reinforced concrete beams strengthened with textile reinforced concrete. *J. Civ. Eng.* **2011**, *44*, 23–34.
42. Ai, S.X.; Yin, S.P.; Xu, S.L. Research progress and application of textile reinforced concrete. *J. Civ. Eng.* **2015**, *48*, 27–40.
43. Yin, S.P. Research on Basic Mechanical Properties of TRC and Flexural Behavior of Reinforced Concrete Beams. Ph.D. Thesis, Dalian University of Technology, Dalian, China, 2010.
44. Yin, S.P.; Xu, S.L.; Wang, F. Bonding and lap bonding properties of woven fiber webs in fine-grained concrete. *J. Build. Mater.* **2012**, *15*, 34–41.

45. Xu, S.L.; Yin, S.P. Study on the normal section bearing capacity of RC flexural members strengthened with fiber woven mesh reinforced fine-grained concrete. *J. Civ. Eng.* **2012**, *45*, 1–7.
46. Xu, S.L.; Yin, S.P.; Cai, X.H. Study on crack resistance of reinforced concrete flexural beams strengthened with textile reinforced concrete. *Hydraul. J.* **2010**, *41*, 833–840.
47. Yin, S.P.; Xu, S.L. Tensile mechanical model of textile reinforced concrete[J]. *Acta Mater. Compos. Sin.* **2012**, *29*, 222–229.
48. Li, H.; Xu, S.L. Study on mechanical properties of textile reinforced concrete thin plate. *J. Build. Struct.* **2007**, *4*, 117–122.
49. Yin, S.P.; Shen, J.; Jia, S. Experimental study on fatigue failure of reinforced concrete beams strengthened with textile reinforced concrete. *J. Build. Struct.* **2015**, *36*, 86–92.
50. Xu, S.; Shen, L.; Wang, J.; Fu, Y. High temperature mechanical performance and micro interfacial adhesive failure of textile reinforced concrete thin-plate. *J. Zhejiang Univ. Sci. A Appl. Phys. Eng.* **2014**, *15*, 31–38. [CrossRef]
51. Xun, Y.; Yin, H.Y.; Xiao, B.H. Experimental study on shear capacity of RC beams strengthened with textile reinforced concrete. *J. Civ. Eng.* **2012**, *45*, 58–64.
52. Liu, D.J.; Huang, H.W.; Xue, Y.D.; Wang, M.Z. Study on mechanical properties of tunnel lining reinforced by fiber woven mesh reinforced concrete. *Eng. Mech.* **2014**, *31*, 91–98 + 111.
53. Sun, W.; Zhang, Y.M.; Yan, H.D.; Mu, R. Damage and damage resistance of high strength concrete under the action of load and freeze-thaw cycles. *Cem. Concr. Res.* **1999**, *29*, 1519–1523. [CrossRef]
54. Mu, R. Durability and Life Prediction of Concrete under the Combined Action of Freeze-Thaw Cycle, External Bending Stress and Salt Solution. Ph.D. Thesis, Southeast University, Nanjing, China, 2000.
55. Li, C.C. Experimental Study on Durability of FRP Reinforced Concrete Structures. Ph.D. Thesis, Dalian University of Technology, Dalian, China, 2006.
56. Bai, Z.L. Research on Flexural Properties of Fiber Woven Mesh Reinforced Concrete under Freeze-Thaw Cycles. Master's Thesis, Jilin University, Changchun, China, 2022.
57. Yan, W.J.; Niu, F.J.; Wu, Z.J.; Niu, F.H.; Lin, Z.J.; Ning, Z.J. Mechanical properties of polypropylene fiber reinforced concrete under freeze-thaw cycles. *Transp. Eng. J.* **2016**, *16*, 37–44.
58. Cao, D.F.; Ge, W.J.; Guo, R.Y.; Yuan, S.F.; Wang, B.Y. Experimental study on flexural behavior of reinforced concrete beams after freeze-thaw cycles. *J. Build. Struct.* **2014**, *35*, 137–144.
59. Ge, W.; Ashour, A.F.; Lu, W.; Cao, D. Flexural Performance of Steel Reinforced ECC-Concrete Composite Beams Subjected to Freeze–Thaw Cycles. *Int. J. Concr. Struct. Mater.* **2020**, *14*, 11. [CrossRef]
60. Murali, G.; Vinodha, E. Experimental and Analytical Study of Impact Failure Strength of Steel Hybrid Fibre Reinforced Concrete Subjected to Freezing and Thawing Cycles. *Arab. J. Sci. Eng.* **2018**, *43*, 5487–5497. [CrossRef]
61. Tian, J.; Wu, X.W.; Zheng, Y.; Du, Y.; Quan, X. Experimental study and mixed-dimensional FE analysis of T-rib GFRP plate-concrete composite bridge decks. *Adv. Mater. Sci. Eng.* **2018**, *2018*, 7531912. [CrossRef]
62. Ministry of Housing and Urban-Rural Development of the People's Republic of China. *GB/T50082-2009*; Test Method for Long-Term Performance and Durability of Ordinary Concrete. China Construction Industry Press: Beijing, China, 2010.
63. Zhang, Y.; Zhang, S.; Jiang, X.; Zhao, W.; Wang, Y.; Zhu, P.; Yan, Z.; Zhu, H. Uniaxial tensile properties of multi-scale fiber reinforced rubberized concrete after exposure to elevated temperatures. *J. Clean. Prod.* **2023**, *389*, 136068. [CrossRef]
64. Zhang, Y.; Zhang, S.; Zhao, W.; Jiang, X.; Chen, Y.; Hou, J.; Wang, Y.; Yan, Z.; Zhu, H. Influence of multi-scale fiber on residual compressive properties of a novel rubberized concrete subjected to elevated temperatures. *J. Build. Eng.* **2023**, *65*, 105750. [CrossRef]
65. Zhang, Y.; Zhang, S.; Jiang, X.; Chen, Q.; Jiang, Z.; Ju, J.W.; Bauchy, M. Insights into the thermal effect on the fracture toughness of calcium silicate hydrate grains: A reactive molecular dynamics study. *Cem. Concr. Compos.* **2022**, *134*, 104824. [CrossRef]
66. Zhang, Y.; Zhou, Q.; Ju, J.W.; Bauchy, M. New insights into the mechanism governing the elasticity of calcium silicate hydrate gels exposed to high temperature: A molecular dynamics study. *Cem. Concr. Res.* **2021**, *141*, 106333. [CrossRef]